WARWICK
THE UNIVERSITY OF WARWICK

Original citation:
Spooner, Stephen, Assis, Andre N., Warnett, Jason, Fruehan, Richard J., Williams, M. A. (Mark A.) and Sridhar, Seetharaman (2015) CSLM, XCT Couple interrogation of the emulsification interaction between free steel droplets suspended in steel making slags. In: CTSSC-EMI Symposium, Tokyo, Japan, 3-4 Sep 2015.

Permanent WRAP URL:
http://wrap.warwick.ac.uk/80858

Copyright and reuse:
The Warwick Research Archive Portal (WRAP) makes this work by researchers of the University of Warwick available open access under the following conditions. Copyright © and all moral rights to the version of the paper presented here belong to the individual author(s) and/or other copyright owners. To the extent reasonable and practicable the material made available in WRAP has been checked for eligibility before being made available.

Copies of full items can be used for personal research or study, educational, or not-for-profit purposes without prior permission or charge. Provided that the authors, title and full bibliographic details are credited, a hyperlink and/or URL is given for the original metadata page and the content is not changed in any way.

A note on versions:
The version presented here is a working paper or pre-print that may be later published elsewhere. If a published version is known of, the above WRAP URL will contain details on finding it.

For more information, please contact the WRAP Team at: wrap@warwick.ac.uk

warwick.ac.uk/lib-publications

CTSSC-EMI Symposium

CSLM, XCT Couple Interrogation of the Emulsification Interaction between Free Steel Droplets Suspended in Steel Making Slags.

Stephen Spooner[1], Andre N. Assis[2], Jason Warnett[1], Richard Fruehan[3], Mark A. Williams[1], Seetharaman Sridhar[1]

1. University of Warwick, Coventry, UK
2. Previously Carnegie Mellon University, now Vallourec Star
3. Carnegie Mellon University, Pittsburgh, PA, USA

Abstract:

Small Fe-based droplets have been heated to a molten phase suspended within a slag medium to replicate a partial environment within the Basic Oxygen Furnace (BOF). The confocal scanning laser microscope (CSLM) has been used as a heating platform as it offers the high heating rates necessary for slag and metal to become molten in close time proximity avoiding gradual equilibration during heating. The effect of impurities and their transfer across the metal/slag interface, on the emulsification of the droplet into the slag medium was then examined through X-ray Computer Tomography (XCT) scanning of the quenched sample. This gives the mapping of emulsion dispersion in 3D space, calculating the changing of interfacial area between the two materials, and changes of material volume due to material transfer between metal and slag. Samples were then sectioned and radial chemical analysis is used to identify component surface enrichment or lack thereof. Replication of the previously reported study by Assis *et al*[1] has also been carried out, to show repeatability of the experimental set up and conditions through different users.

Introduction:

Many steps in the process of steel making rely on the transfer of impurities from metal to slag; a few examples are silica removal in the blast furnace[2], sulfur in the desulfurization pre-treatment[3], and phosphorus removal in the basic oxygen furnace (BOF)[4]. In the case of phosphorus refining in the BOF, much work has been carried out on the thermodynamic equilibrium between the metal and slag[5–7], giving evidence to the kinetic inhibition of the potential partition possible[8]. This lack of equilibrium could either be caused by lack of homogeneity in the slag layer of the BOF, (reducing the local driving force for phosphorus partition into the slag), or through kinetic restrictions through a deficiency of required interface for refining to transpose across/mass transfer controlling delivery of impurities to the interface[8–10]. Due to the inherent high temperatures the transfer of material at the interface tends to be fast in comparison to the kinetically restricting mass transfer of materials in their respective bulk phases[8–10]. Current level of understanding has extended beyond equilibrium conditions to include the description of mass transport in the slag and metal phases[11–14]. It is however known that under dynamic conditions the interface between phases can display significant perturbation in comparison to a relaxed planar state, and may even lead to emulsification[15–20]. A proper description of the slag/metal reaction necessitates an elucidation of the dynamic change of

interfacial area and the coupling of this change to the interfacial reactions. As such this work intends to investigate the effects of refining performance on interface morphology between Fe alloys and slags where "mixing" of phases may intrinsically occur to reduce the kinetic restrictions of mass transfer.

In this study the specific case of the transient interface in the BOF emulsion phase is considered, which has previously been attributed to offering large contributions to the overall refining performance seen within the BOF[21]. The emulsion phase of the BOF is a mix of slag, gas (O_2, CO/CO_2) and metal droplets caused by the impinging oxygen jet delivered to the bulk bath surface; overcoming the surface tension of the molten metal and sheering material away to form discrete droplets (as well as larger plumes of metal)[22,23].

The interface of metal and slag in this emulsion phase consists of several factors:

1. Amount of metal in the emulsion
2. How long the metal stays in the emulsion (average residence time)
3. The size of discrete metal droplets
4. The morphology of metal droplets

Previous studies, including that of the present authors have investigated the macroscopic elements (point 1 & 2 above) of this interface. Reported residence times ranging from 0.4-120 seconds are given, with an average of around 40 seconds[24–30]. The amount of metal in the emulsion has been reported in a complete range up to 50% of the tap weight dependant on blow time[31,32].

With regards to the kinetics of a specific metal droplet in the emulsion several authors have investigated variable aspects (point 3 & 4 above). Studies have been carried out both on industrial scale and laboratory scale on the size of quenched static samples; these results as well as how they were obtained are shown in *Table 1*.

Table 1. A summary of the previous findings of metal droplet size in oxygen steelmaking emulsions.

Researchers	**Place of collection**	**Droplet Size Range (μm)**
IMPHOS[33]	Inside pilot converter, special lance	16-6360
Resch[34]	Paused and tilted converter	50-2000
Tokovoi *et al*[35]	Upper slag/metal emulsion	1000-2500
Cicutti[21]	Inside full converter, special lance	230-3350
Koria *et al*[36]	Slashed liquid outside crucible	40-70,000
Baptizmanskii *et al*[37]	Cutting hole in crucible wall	50-18000
Meyer[38]	Through tap hole, outside converter	150-3320
Block *et al*[39]	50-150mm above bulk bath inside converter	500 – 4000
Urquhart *et al*[40]	Inside full converter, special lance	63 - 2000

More recently work has begun into the tracking of a droplets transient morphology during refining processes. An example in this area is the work conducted by Rhamdhani *et al*[18] where Fe-A droplets were immersed in CaO-SiO_2-Al2O3, the recovered metal droplets were then measured using a system of paper standards covering the droplet surface, giving an effective but rudimental method of calculating the change in surface area. X-ray fluoroscopy and direct observation of in-situ droplets has also given evidence to the change in droplet shape during Fe alloy/slag interactions[16,41–43]. It has

been proposed by these studies that the initial driving force is integral when evaluating the change in droplet morphology as interfacial tension between the two mediums decreases rapidly allowing for interfacial area increase.

The use of microscopy is perhaps the most essential tool for investigative material science offering the ability to discern micro-structures at finer and finer scales; but usually *a posteriori* to as process. Tools to image evolving micro-structures at steelmaking temperatures and short transient times were not available. Professor Toshihiko Emi pioneered the use of laser confocal optics with an Au-image furnace allowing for in-situ imaging, and his group at Tohoku University where the first to document the clustering of inclusions[44,45], peritectic solidification[46] and particle pushing[47].

The present work, inspired by Prof. Emi's stellar publications, leads on from the initial findings of Assis *et al*[1], where high temperature-confocal scanning laser microscopy (HT-CSLM), and micro x-ray computer tomography (XCT) were coupled together to provide insight into the full transient morphology of an Fe-P 0.2% alloy droplet submerge in slag similar to that seen in end blow BOF refining. Where HT-CSLM was used to provide a high heating rate reaction platform and XCT was used to offer 5 micron resolution 3D quantification of the metal-slag interface of quenched samples.

Initially a repeat of the previously reported work has been carried out to offer consideration to the consistency of the intricate technique used to produce the samples required. This has been followed by initial chemical analysis of the samples from the previous study[1]. The result of which indicate the need of a further trial, where no phosphorus was present, leading to the exploration of oxygen transition across the interface causing spontaneous emulsification.

Experimental:

The experimental set up consists of a Confocal Scanning Laser Microscope (CSLM), used for its high heating and cooling rates. This is followed by X-ray computer tomography (XCT) to give 3D representations of an entire sample. XCT also allows for identification of a representative slice through a sample that can then be sectioned along, polished and chemical analysis performed. The chemical analysis techniques used are: Inductively coupled plasma – mass spectrometry (ICP-MS), wavelength dispersive spectroscopy – scanning electron microscope (WDS-SEM), laser ablation – inductively coupled plasma mass spectrometry (LA-ICPMS), and secondary Ion mass spectrometry (SIMS).

Materials & Methods:

The material used in the initial study has been reported previously[1]. In summary, it consists of a Fe-0.2wt% P alloy, which was reacted with a slag whose XRF Chemical analysis can be seen in *Table 3*, this will be called S1

A repeat of the system described by Assis *et al*, has been conducted. An Fe- 0.2wt % alloy droplet of 17mg ± 0.4mg with a cylindrical input geometry of 1.19mmH 1.49mmD is used (the alloy has the exact same composition as used in the initial study, seen in *Table 2*). This will be called alloy1 (a1). A master slag of the composition seen in *Table 3* (analysis via XRF) was prepared under shield gas argon in an induction furnace at 1600^{o}C from the stock materials, CaO, SiO_2, MgO, Fe_2O_3 and $Ca_2P_2O_7$, this will be called S2.

The second set of material used consists of a 2mm diameter iron wire supplied by Alfa Aesar, cut into discs using a low speed diamond blade saw. This will be called alloy 2 (a2), the composition of which can be seen in *Table 2*. The weight of the resulting discs was between 14 to 16 mg. A master slag for this was prepared with the same reagent grade powders as previously stated inside an MgO crucible, melted for 1600^{o}C for 2hours in a tube furnace under high purity argon to ensure homogeneous mixing. The crucible was then grinded, slag pulverized and analysed via XRF (the composition can be seen in *Table 3*). This will be called S3.

Table 2. ICP detected chemical composition of Fe- alloys used in this study.

	%Mn	%P	%Ni	%Cr	%Al	%C	%S	%O	%N
a1	0.011	0.201	0.003	0.002	0.002	0.0008	0.0012	0.0737	0.0005
a2	0.0003	0.0004	0.0001	0.0003	0.0005	0.004	<0.001	0.0034	<0.001

Table 3. XRF detected chemical composition of master slags, used in this study and by Assis et al.

	%CaO	%MgO	%SiO_2	%FeO_t	%P_2O_5	Cao/SiO_2
S1	36.64	7.08	16.98	33.56	1.66	2.16
S2	36.89	7.14	16.21	32.31	1.65	2.28
S3	38.15	10.26	16.89	34.70	0.01	2.26

High Temperature Confocal Scanning Laser Microscope (HT-CSLM):

MgO crucibles (9mmD, 4.5mmH) were packed with 0.45 g ± 0.06g of the respective master slag. The crucible was then loaded into the HT-CSLM, and the chamber cycled 3 times for ten minutes each through vacuum and argon back filling (99.9999% argon). The slag was pre-melted at 1625^{o}C for 30s and then cooled at a nominal rate of 1000^{o}C min^{-1} with helium gas. The crucible is then removed from the chamber and a droplet is loaded into the centre of the slag meniscus surface. A further 0.15g ±0.042g of slag powder hand pressed on top to ensure the droplet will be submerged when in liquid state. The entire sample was reloaded, cycled again, and the experiment is then run following the regime shown in *Table 4*, under 200 ml min^{-1} argon flow. Steps 1 and 4 are required to reduce the chance of damaging the bulb.

Table 4. Heating and quenching regime of all samples. ## being the period of time a sample was held at high temperature for.

	Step 1	Step 2	Step 3	Step 4
Temp (K)	Rt-373.2	373.2->1873.2	S1873.2->773.2	773.2->Rt
Heating Rate (K min^{-1})	50	500	-1200	-300
Hold Time (s)	45	##	70	-

X-ray Computer Tomography:

Samples containing S1 and S3, were scanned using a 'Nikon Metrology XT H 320 LC' CT scanner and samples containing S2 were scanned using a 'Zeiss Versa 520'. The difference in machines was due to availability during experiments, with the Zeiss preferred due to its better signal to noise ratio

within images. This arises from different source and detectors within the systems, and a smaller source/detector distance in the Zeiss machine that is better suited for higher resolution tomography

The Nikon machine consists of a 225kV micro focus with tungsten reflection target and a flat panel detector consisting of 2000x2000 pixels, each of 200 microns in size. The Zeiss machine has a 160kV micro focus source with an alumina transmission target and ca charge-couple device based detector 2000x2000 pixels, with a size dependant on the optic used (x0.4 optic was used in this study with 1.75 micron pixel size).

The parameters for each scan are shown in *Table 5*. The scans were then reconstructed in proprietary packages included within the systems that use filtered back projection. The reconstructed 3D volume was then evaluated in 'VGStudio MAX' (Volume Graphics GmbH. Germany). Further information on the CT scanning including reference pieces used for scaling, determination of the droplet isosurface and validation of the scanning parameters can be found in previous works[1,48].

Table 5. Parameters used within the two scanners. *There is an additional focusing step performed by an optic in the Zeiss machine, where x0.4 was used in this study

	Nikon	Zeiss
Voltage (kV	220	140
Power (W)	3.1	10
Exposure	4	3
Projections	3142	3142
Filter (mm)	Cu 0.5	CaF_2 1.0
Magnification	x39.5	*x6.69
Voxel Size	5.06	4.90

Chemical Analysis:

In order to evaluate the phosphorus content in the metal before and during emulsification for system 1 samples, Wavelength Dispersive Spectroscopy (WDS-SEM), Laser Ablation ICP-MS (LA-ICPMS) and Secondary Ion Mass Spectroscopy (SIMS) were used. Each of these techniques has the advantage of having small spot sizes which make it possible to chemically analyse the metal drop and emulsion.

WDS-SEM was the initially selected tool to analyse of the phosphorus content in the metal drops as it is a non-destructive technique and relatively simple to use. WDS offers better peak resolution and separation than EDS and can potentially detect concentrations below 1wt.% with the usage of proper standards. Unlike EDS, the detector reads and counts x-rays generated of a single wavelength at a time that are diffracted by a crystal of proper lattice spacing. In the present study the standards used were pure Fe and GaP for iron and phosphorus respectively. Each of the standards was used to standardize accelerating beam voltages of 25 and 30kV with spot sizes of 6 and 7 microns. The high accelerating voltages and bigger spot sizes were necessary in order to achieve the highest beam current possible in the SEM, which helps in quantifying low concentrations.

LA-ICPMS differs from regular ICP-MS in that it uses a focused laser beam to ablate a small area of the sample. This technique was used to confirm the data acquired by WDS and only one sample was

analysed via this technique. A total of four measurements were taken using ICP-MS across different regions of the metal drop. Each “shot” ablated roughly 5µm in depth with a spot size of 100µm in diameter.

SIMS was used for the analysis of oxygen in the 20s sample. SIMS uses a focused ion beam to sputter the surface of the sample. As the ion beam “mills” the surface, secondary ions are generated and these ions are analysed by a mass spectrometer. Quantification was based on a stainless steel 302 standard.

Results and Discussion:

The interaction of metal droplets with slag has been interrogated via the CT scanning of quenched samples produced in the HT-CSLM. The first series reported by Assis *et al* (ref), has now undergone initial chemical analysis of representative sectioned surfaces (a1 and S1, system 1). Secondly a repeat of these initial conditions has been completed, to interrogate the consistency of the previously reported tomography results (a1 and S2, system 2). Finally, as a response to the initial chemical analysis of system 1, a low phosphorus system has been created and analysed to investigate the cause of emulsification (a2 and S3, system 3).

Repeatability of emulsification experiments interrogation:

XCT scans of quenched samples for a system (system 2) designed to be a repeat of that used by Assis *et al* (system 1) have been reconstructed to produces images seen in *Figure 1*. It can be seen from *Figure 1* that emulsification of the droplet in S2 has occurred.

Several points should be taken from these initial images that display significant differences from the original study. Firstly, the holding times of these samples crosses over, and extends beyond that of the originals (0-120seconds). This was because the present samples were run on a different HT-CSLM and by a different user; this resulted in a diverted regime, where it was found the droplet was taking longer to melt than seen before. *Figure 2* shows the images of initial trials within the time period of Assis *et al's* samples[1]. It can be seen that in the 30 and 60 second sample the droplet has still

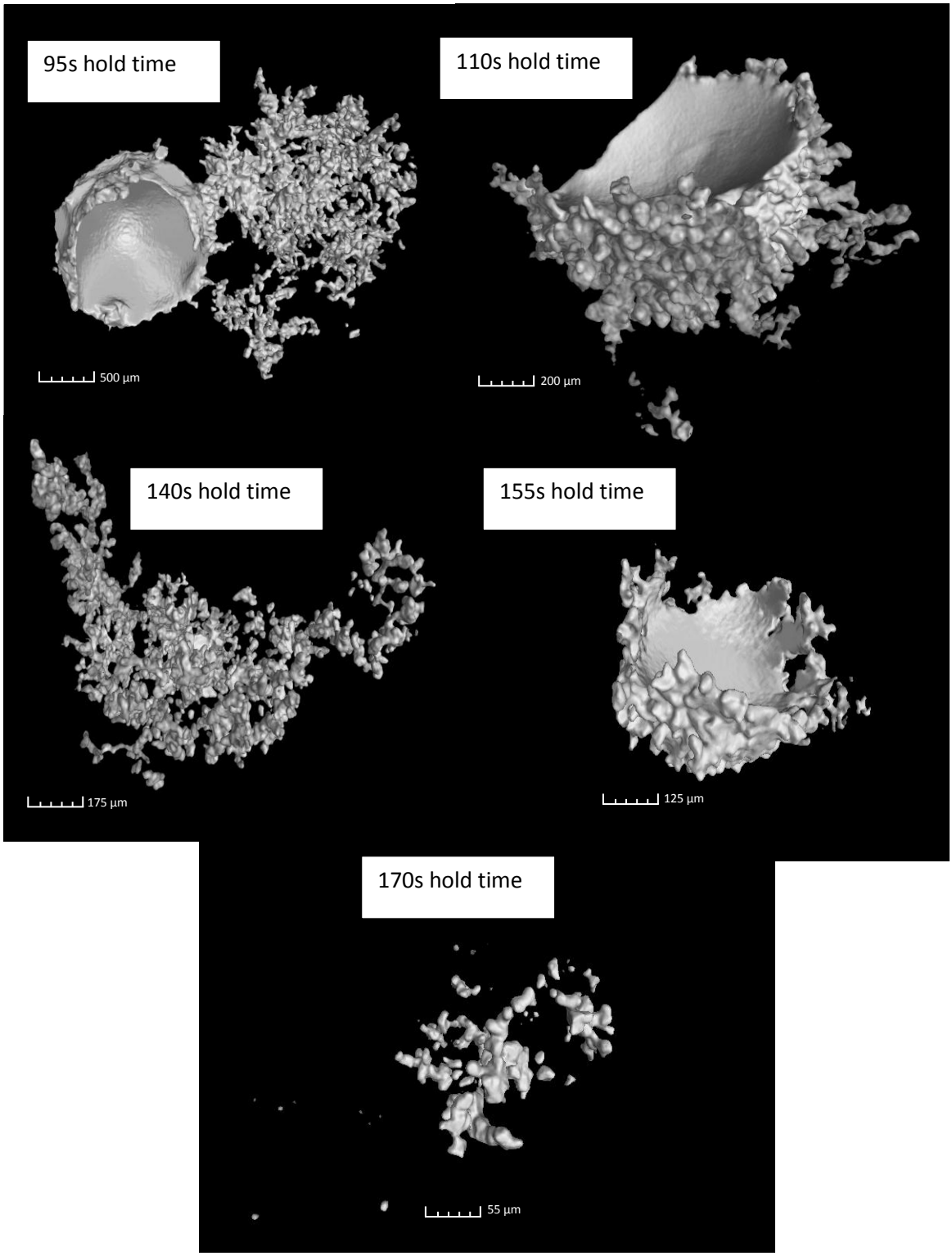

Figure 1. Reconstructed images from XCT scanning, only showing the metal droplet.

maintained significant portions of the original cylindrical geometry. At 90 seconds the sample is molten with a spherical geometry, and the surface can be seen to have begun to roughen, either through the starting of initial emulsification, or due to the shrinkage of the droplet in an uneven manner during quenching Figures 2 a) – C) display a cross section of the entire crucible, showing droplet vertical location, and the clear distinction between droplet and slag. It should be noted from the images, the darkest areas reveal porosity through the slag medium; most of the porosity can be

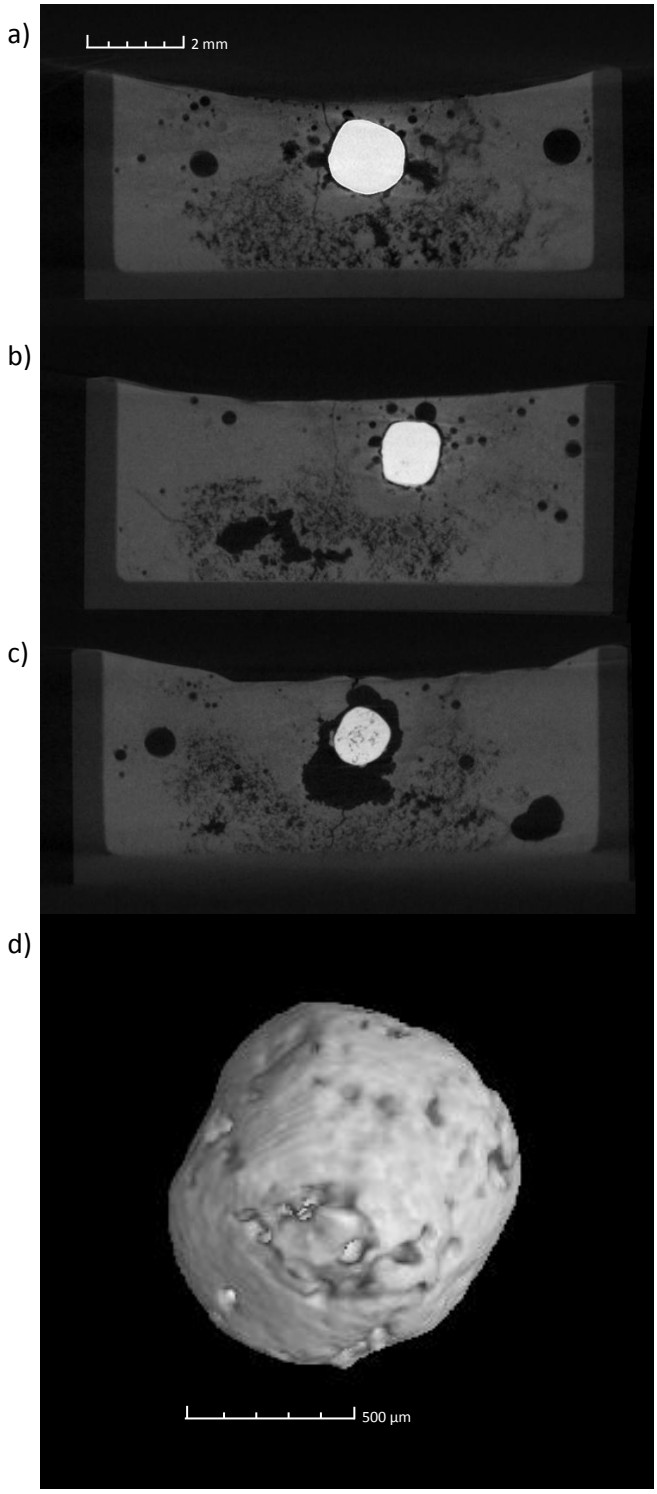

Figure 2. 2D section of XCT scans showing droplet morphology during hold times within the previous stud's times. a) 30s, b) 60s, c)90s, d)higher magnification 3D image of 90 second sample.

accounted for due to shrinkage during quenching, however some porosity would also be caused by trapped gasses due to reduction in gas solubility when material is cooled, and minor side reactions.

The next observation is the pathway of emulsification to coalescence is seen to differ significantly from system 1. This is thought to be due to the slower heating rates seen within system 2. A slower heating rate will have caused slag and metal to become molten at further time separation. This will potentially reduce the initial driving force of partition equilibration, as material will begin to exchange before the droplet is fully molten. Due to this slower heating rate and the need to hold material at high temperature for longer periods of time, the amount of droplet dissolved into the slag could greatly increase. There are two proposed pathways for system 2:

1. The droplet reaches molten state slowly, with initial refining taking place (90s), emulsification begins with half the droplet breaking away (95s), this break away is either dissolved or reduces in size below the resolution of CT scanning (110s), the remaining sample continues to emulsify (140s), and then coalesces (150s). Finally the sample continues to be dissolved into the slag reducing visible material (170s).
2. Up to 90 seconds the same behaviour, full emulsification where some of the sample pools back together due to gravity effects through porous areas (95s), emulsification continues through to 155 seconds (with pooling due to porosity in the slag happening in 110s and 155s samples). Finally after 170s large amounts of the sample have either dissolved or dispersed below CT resolution.

The pooling theory is due to the seen orientation of the half domed sections of the sample, where the cup faces upwards, and has large areas of porosity seen above (see *Figure 3*). Any emulsified material here would have dropped/have no support to be separated under quenching conditions.

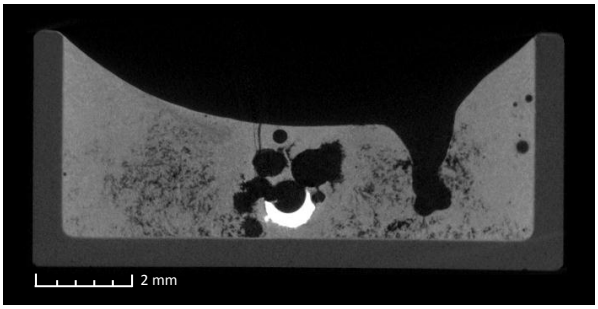

Figure 3. 2D slice of 95 second sample showing the orientation of the domed part of the sample.

Finally it can be observed that a large amount of material is being lost through the reaction time (briefly mentioned in the previous point). At this stage, the two options are either emulsification beyond the resolution of the current CT scans, or dissolving of the Fe-P droplet into the slag medium. Due to time retrains the authors are unable to support either of these ideas, in the future higher resolution CT scanning and SEM imaging will be used to investigate the presence of smaller particles. XRF analysis of the slag may also be carried out to investigate if the Fe content has increase.

Chemical analysis of system 1:

As previously mentioned, WDS-SEM and LA-ICPMS were used for phosphorus analysis while SIMS was used for oxygen analysis. A total 5 "shots" were made close to the centre of the metal drop. Each shot milled roughly 10µm in depth with a spot size of 30µm. A sixth oxygen measurement was performed using SIMS to generate a depth profile of the oxygen concentration. This profile was obtained by milling from the centre of the cross-section of the droplet towards the interface of the droplet. This profile is shown in *Figure 4* . The summary of chemical analysis carried out by each technique is shown in *Table 6*.

Table 6. Summary of chemical analysis performed using the various techniques described.

	(wt.% P)			(wt. %O)	
Reaction Time (s)	**ICP-MS**	**WDS-SEM**	**LA-ICPMS**	**LECO**	**SIMS**
Original alloy	0.201	0.170±0.032		0.0737	
0		0.179±0.015			
10		0.002±0.002			
20		0.008±0.005	0.0019±0.0001		0.213±0.139
30		0.003±0.002			

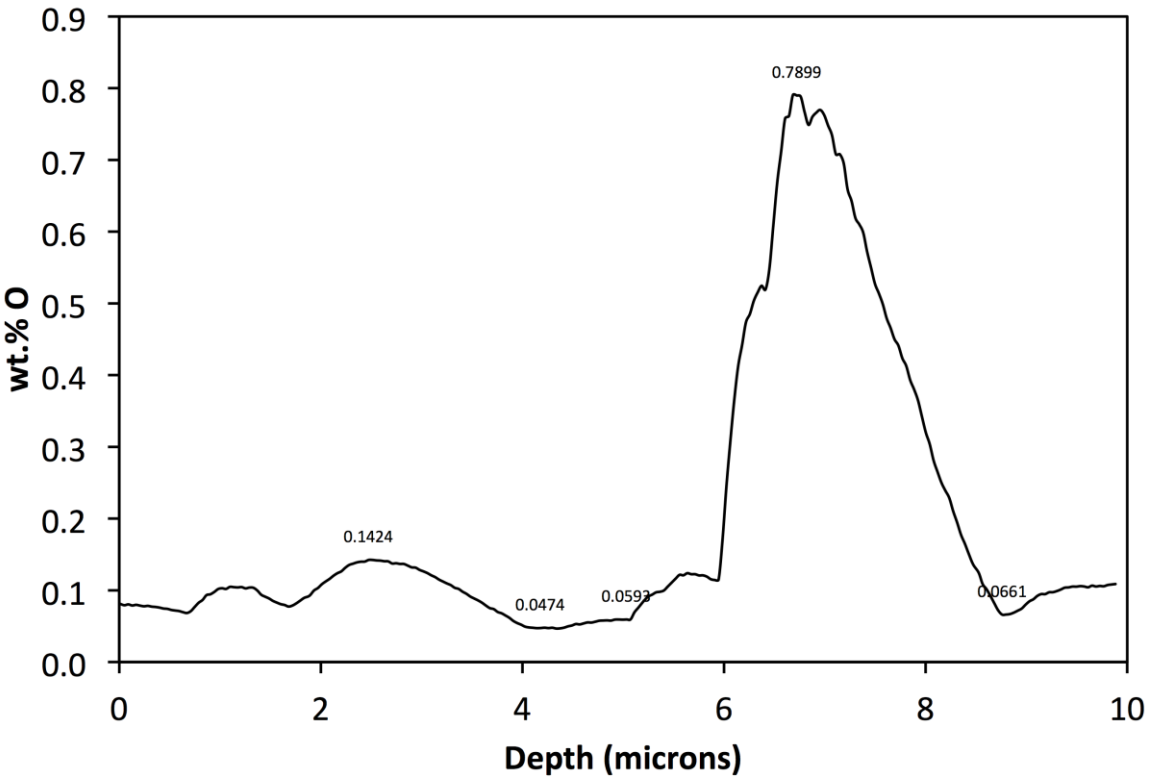

Figure 4. Measured oxygen concentration as a function of depth into the 20s sample (using a cross section) from Assis et al.

The results mapped against the previously reported surface area profiles of the samples (Ai/A0) show phosphorus had been removed from the droplet before 10s of reaction time (see *Figure 5*). This was much sooner than the first visualisation of emulsification in system 1, at 30 seconds. This leads to the conclusion phosphorus exchange across the interface is not the reason for

emulsification to occur, and the equilibration time for phosphorus between metal and slag is much shorter than the ideal predicted time of 120 seconds calculated previously[1].

SIMS results showing a large increase in oxygen concentration within the droplet at 20 seconds, as compared to the initial alloy (whose oxygen analysis was outsources to LECO). The Fe-FeO equilibrium based on activity of FeO in the master slag has been predicted using FactSage, giving oxygen equilibrium content within the metal of ~1000ppm. This coupled with the calculated reduction in oxygen early on due to reaction with phosphorus gives the predicted oxygen content as a function of time mapped in *Figure 5*. SIMS analysis showed an average oxygen content of 0.213±0.139 wt.%, significantly higher than the predicted equilibrium, *Figure 4* also shows the heterogeneous distribution of oxygen radially through the droplet, with values from below equilibrium to those much higher. SIMS does not offer quantified data, however should be within a factor of 2 when appropriate standards are used.

From the points mentioned above, it is hypothesised that the exchange of oxygen across the metal/slag interface is the cause of emulsification. It is not known what would cause the mass oversaturation of oxygen within the droplet, however the mass transfer of oxygen back into the slag to reach equilibrium between 20-30 seconds, would be rapid. This along with the known fact oxygen is a surfactant in a metal/slag system, leads the authors to presented hypothesis.

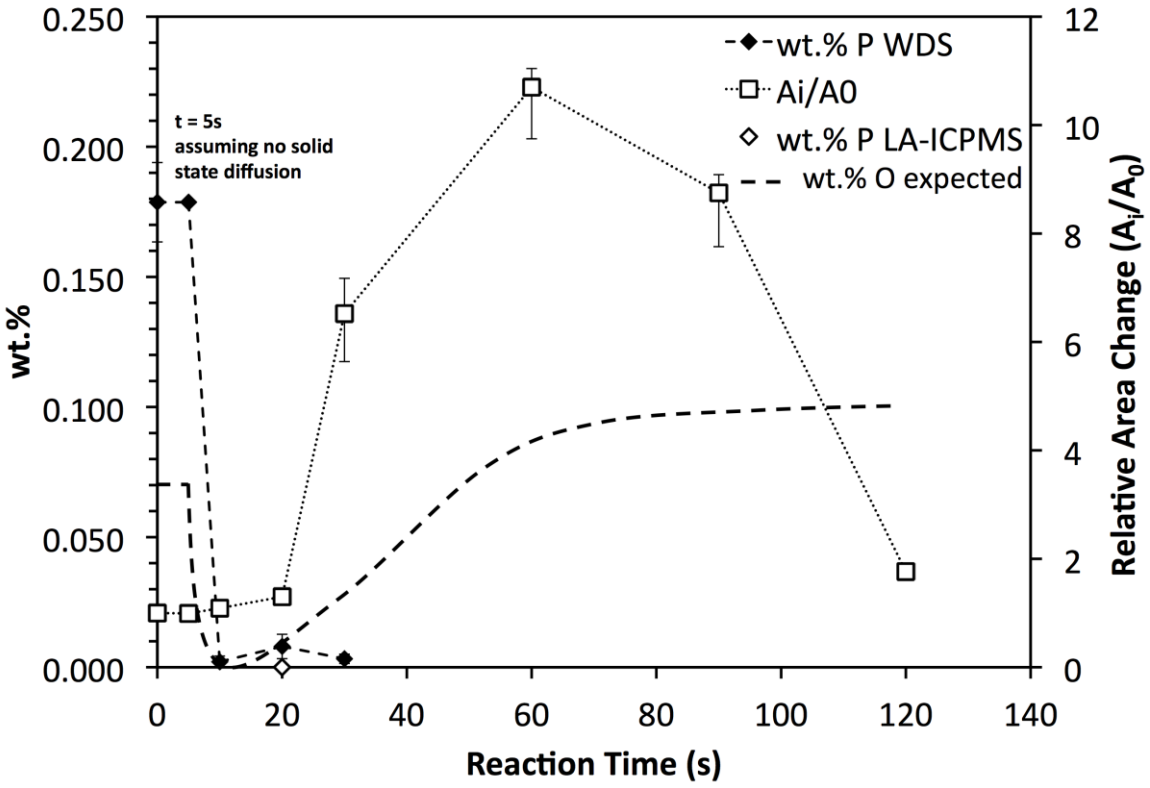

Figure 5. Expected oxygen concentration profile as a function of reaction time (LA-ICPMS only available at 20s).

In addition to the material presented, it was found that the cross sectioned 0s sample contained a dispersion of particles throughout the droplet (see *Figure 6*). Local WDS of these particles showed them to be significantly higher in phosphorus than the bulk material (from 1.7-3.1 wt.% P). These particles were not seen in the cross sectioned images of later samples, where the phosphorus levels were seen to be drastically reduced (10s onwards). Several images of the particles were used to calculate an area fraction of 0.4%, with this and the average particle concentration the amount of phosphorus removed is still significantly greater. The authors intend to interrogate this further in order to define a realistic mechanism for phosphorus removal.

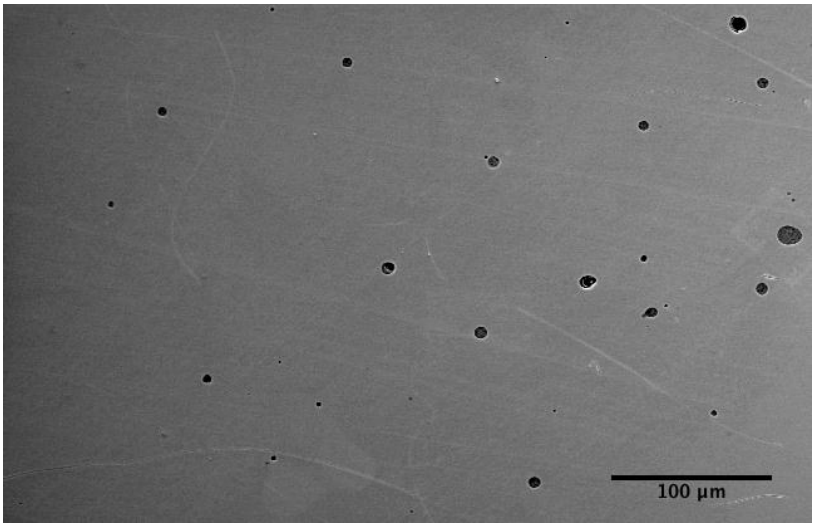

Figure 6. Low magnification SEM picture of 'P-rich' particles.

System 3, dynamic changes in surface area:

3D reconstructions of XCT scans performed on system 3 quenched samples are shown in *Figure 7*. The initial sample of 10s was selected as the starting point as this was when samples were shown to be fully liquid from system 1[1] and used the sample set up and user as previously, other sample times were selected in order to try and capture comparative emulsification data as to the initial study.

The surface area and volume of the droplets in system 3 samples were determined as described previously[1], the results of which are shown in *Table 7* and *Table 8* respectively. The min, max and selected surface areas/volumes are based on manual selection of grey values.

Table 7. Raw data for surface area measurements of system 3.

Time (s)	Surface Area Selected (mm^2)	Surface Area Max (mm^2)	Surface Area Min (mm^2)	Ai/A0
10	6.60	6.60	N.A	1.00
30	8.37	8.38	8.36	1.27
60	6.84	6.86	6.83	1.04
90	65.75	73.69	58.13	9.96

Table 8. Raw data for volume measurements of system 3.

Time (s)	Volume Selected (mm^3)	Volume Max (mm^3)	Volume Min (mm^3)	Vi/V0
10	1.29	1.30	1.28	1
30	1.31	1.32	1.30	1.02
60	1.19	1.19	1.18	0.92
90	0.96	1.10	0.83	0.74

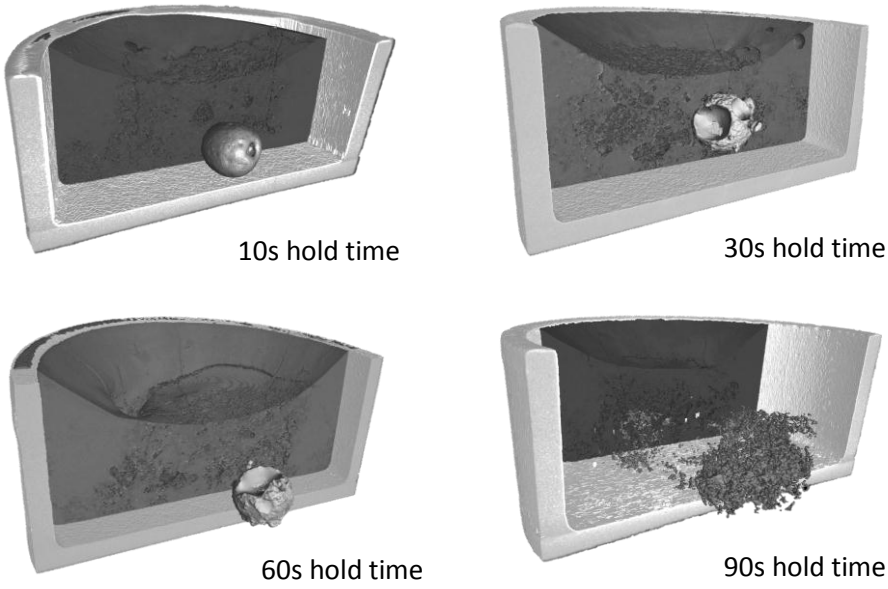

Figure 7. Metal droplet 3D spatial geometry for different holding times in system 3.

It can be seen the 10 second sample has melted and acquired a spherical shape, and emulsification takes place between 60 and 90 seconds. From table#.## the surface area of the drop stay relatively constant through the first 3 samples 6 – 8 mm^2, followed by an increase by an order of magnitude to 65.75 mm^2. This increase in area is very similar to that seen in the previous study[1]; however there is a delay of ~30 seconds. This is clearly seen in the normalized area curves displayed in *Figure 8*. In system 3, oxygen in transferred from the slag into the metal, and the result appears to validate the hypothesis of oxygen transfer across the interface being responsible for the spontaneous emulsification (the behaviour should occur regardless of oxygen transfer direction). The delay of 30 seconds, may be as a product of the fact no phosphorus exchange occurs in comparison to system one, however it may also be due to aspects such as inconsistent heat transfer inside the HT-CSLM, or other parameters that effected the differences seen in system 2.

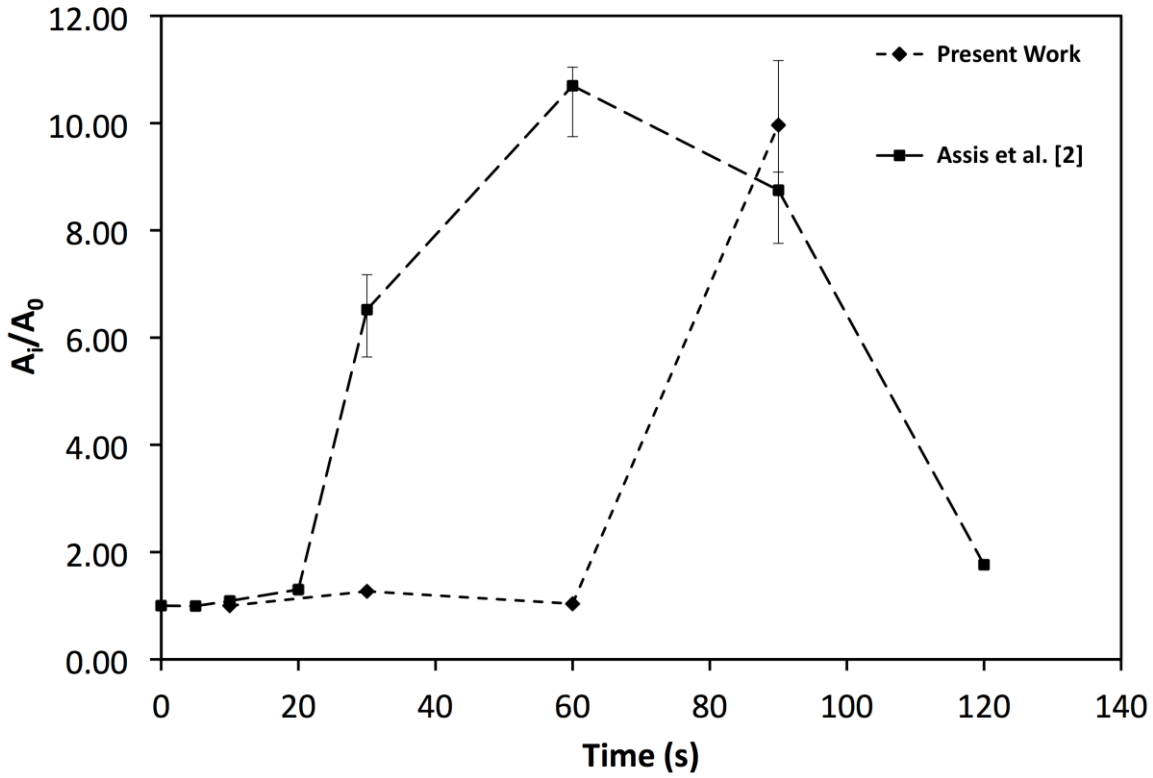

Figure 8. Normalized surface area of metal droplets as a function of time, for system 3 where oxygen from the slag in entering the droplet, and system 1 where phosphorus from the droplet is being refined to the slag.

Conclusions and Further Work:

Chemical analysis of samples from a previous study by Assis *et al*[1] appear to show phosphorus movement across the interface between a metal drop and slag is not responsible for spontaneous emulsification. Instead it is hypothesised oxygen partition in either direction across the interface causes a drop in interfacial tension through surfactant effects, and active refining. This is supported by a system where only oxygen content was drastically away from equilibrium, showing similar behaviour to that seen previously (apart from a slight delay).

A replication of the previous study has also been carried out by another user with a different HT-CSLM. This showed very different melting times for the metal droplet, and a result changed pathway of droplet morphology through the reaction period. Discussion has been given as to why these differences may have been seen, with heating performance, and sample preparation being the clearest possibilities.

The authors intend to continue this work, with use of optically transparent slags, and Fe-Al alloys, in an attempt to visualise the emulsification *in situ* using the HT-CSLM. The study will also be extended to encompass the effects of other common impurities seen in steel makings, such as carbon and sulfur.

References:

1. Assis, A. N. *et al.* Spontaneous Emulsification of a Metal Drop Immersed in Slag Due to Dephosphorization: Surface Area Quantification. *Metall. Mater. Trans. B* (2014). doi:10.1007/s11663-014-0248-z

2. Gustavsson, J. Reactions in the Lower Part of the Blast Furnace with Focus on Silicon. (2004).

3. Yang, A. A pre-study of Hot Metal Desulphurization. (2012).

4. Basu, S. Studies on dephosphorisation during steelmaking. (2007).

5. Tayeb, M. A., Fruehan, R. & Sridhar, S. Phosphorus partitioning during EAF refining of DRI based steel. in *Int. Symp. Liq. Met. Process. Cast.* 353–358 (2013).

6. Tayeb, M. A., Fruehan, R. & Sridhar, S. De-phosphorization in the DRI-EAF steelmaking and the effect of alumina. in *AISTech* 1 (2014).

7. Sano, N. & Riboud, P. V. *Advanced physical chemistry for process metallurgy*. (Academic Press, 1997).

8. Manning, C. P. & Fruehan, R. J. The rate of the phosphorous reaction between liquid iron and slag. *Metall. Mater. Trans. B Process Metall. Mater. Process. Sci.* **44,** 37–44 (2013).

9. Wei, P., Sano, M., Hirasawa, M. & Mori, K. Kinetics of Phosphorus Transfer between Iron Oxide Containing Slag and Molten Iron of High Carbon Concentration under Ar-O2 Atmosphere. *ISIJ Int.* **33,** 479–487 (1993).

10. Wei, P., Sano, M. & Hirasawa, M. Kinetics of Carbon Oxidation Reaction between Molten. *ISIJ Int.* **31,** 358–365 (1991).

11. Kitamura, S., Saito, S., Utagawa, K., Shibata, H. & Robertson, D. G. C. Mass Transfer of P2O5 between Liquid Slag and Solid Solution of 2CaO·SiO2 and 3CaO·P2O5. *ISIJ Int.* **49,** 1838–1844 (2009).

12. Diao, J., Liu, X., Zhang, T. & Xie, B. Mass transfer of phosphorus in high-phosphorus hot-metal refining. *Int. J. Miner. Metall. Mater.* **22,** 249–253 (2015).

13. Muhmood, L., Viswanathan, N. N. & Seetharaman, S. Some Investigations into the Dynamic Mass Transfer at the Slag–Metal Interface Using Sulfur: Concept of Interfacial Velocity. *Metall. Mater. Trans. B* **42,** 460–470 (2011).

14. Martín, M., Rendueles, M. & Díaz, M. Steel-Slag Mass Transfer in Steel Converter, Bottom and Top/Bottom Combined Blowing Through Cold Model Experiments. *Chem. Eng. Res. Des.* **83,** 1076–1084 (2005).

15. Chung, Y. & Cramb, A. Dynamic and equilibrium interfacial phenomena in liquid steel-slag systems. *Metall. Mater. Trans. B* **31,** 957–971 (2000).

16. Gaye, H. & Riboud, P. V. Oxidation kinetics of iron alloy drops in oxidizing slags. *Metall. Trans. B* **8,** 409–415 (1977).

17. Jakobsson, a., Nasu, M., Mangwiru, J., Mills, K. C. & Seetharaman, S. Interfacial tension effects on slag--metal reactions. *Philos. Trans. R. Soc. A Math. Phys. Eng. Sci.* **356,** 995–1001 (1998).

18. Rhamdhani, M., Brooks, G. & Coley, K. Analysis of interfacial area changes during spontaneous emulsification of metal droplets in slag. *Metall. Mater. …* **37,** 1087–1091 (2006).

19. Rhamdhani, M., Coley, K. & Brooks, G. Analysis of the source of dynamic interfacial phenomena during reaction between metal droplets and slag. *Metall. Mater. …* **36,** (2005).

20. Rhamdhani, M., Coley, K. & Brooks, G. Kinetics of metal/slag reactions during spontaneous emulsification. *Metall. Mater. …* **36,** (2005).

21. C. Cicutti, M. Valdez, T. Perez, J. Petroni, A. Gomez, R. D. and L. F. Study of Slag-Metal Reactions in an LD-LBE Converter. **250,**

22. Sabah, S. & Brooks, G. Splash Distribution in Oxygen Steelmaking. *Metall. Mater. Trans. B* **46,** 863–872 (2014).

23. Sabah, S. & Brooks, G. Splashing in Oxygen Steelmaking. *ISIJ Int.* **54,** 836–844 (2014).

24. Price, D. J. in *Process Eng. Pyrometallurgy* 8–15 (1974).

25. He, Q. & Standish, N. A model study of residence time of metal droplets in the slag in BOF steelmaking. *ISIJ Int.* **30,** 356–361 (1990).

26. Dogan, N., Brooks, G. A. & Rhamdhani, M. A. Comprehensive Model of Oxygen Steelmaking Part 1: Model Development and Validation. *ISIJ Int.* **51,** 1086–1092 (2011).

27. Dogan, N. & Brooks, G. A. Comprehensive model of oxygen steelmaking part 2 : application of bloated droplet theory for decarburization in emulsion zone Comprehensive Model of Oxygen Steelmaking Part 2 : Application of Bloated Droplet Theory for Decarburization in Emulsion Zone. *ISIJ Int.* **51,** 1093–1101 (2011).

28. Kozakevitch, P. Foams and Emulsions in Steelmaking. *J. Miner. Met. Mater. Soc.* **22,** 57–58 (1969).

29. Brooks, G., Pan, Y. & Coley, K. Modeling of trajectory and residence time of metal droplets in slag-metal-gas emulsions in oxygen steelmaking. *Metall. Mater. Trans. B* **36,** (2005).

30. Schoop, J., Resch, W. & Mahn, G. Reactions occurring during the oxygen top blown process and calculation of metallurgical control parameters. *Ironmak. Steelmak.* (1978).

31. Millman, M. S., Overbosch, a, Kapilashrami, a, Malmberg, D. & Brämming, M. Some observations and insights on BOS refining. *Ironmak. Steelmak.* **40,** 460–469 (2013).

32. Millman, M. S., Overbosch, a., Kapilashrami, a., Malmberg, D. & Brämming, M. Observations on BOS refining. *Trans. Indian Inst. Met.* **66,** 525–534 (2013).

33. Millman, M. & Kapilashrami, A. Imphos: improving phosphorus refining. *Publ. Off. …* (2011).

34. Resch, W. Kinetics of P Removal During O Top-Blowing Processes for P-Rich Fe. (1976).

35. Tokovoi, O. K., Stroganov, A. I. & Povolotskii, D. Y. Tokovoi. *Steel USSR* 116–117 (1972).

36. Koria, S. C. & Lange, K. W. Estimation of drop sizes in impinging jet steelmaking processes. *Ironmak. Steelmak.* **13,** 236–240 (1986).

37. V. I. Baptizmanskii, V. B. Okhoskii, K. S. Provirin, G.A. Shcherdrin, Y. A. A. and A. G. V. Investigation of the Physico-chemical Processes in the Reaction Zone with Oxygen Injection of the Metal. *Steel USSR* **7,** p329–331 (1977).

38. Meyer, H. W., Porter, W. F., Smith, G. C. & Szekely, J. Slag-Metal Emulsions and their Importance in {BOF} Steelmaking. *J. Met.* 35–42 (1968).

39. R.F. Block, A. M. and G. S. Physical Processes in the Top Blown Oxygen Converter. *Arch Eisenhuttenwes* **44,** p357–361 (1973).

40. Urquhart, R. C. & Davenport, W. G. Foams and emulsions in oxygen steelmaking. *Can. Metall. Q.* **12,** 507–516 (1973).

41. Min, D. & Fruehan, R. Rate of reduction of FeO in slag by Fe-C drops. *Metall. Trans. B* **23,** 29–37 (1992).

42. Molloseau, C. & Fruehan, R. The reaction behavior of Fe-CS droplets in CaO-SiO2-MgO-FeO slags. *Metall. Mater. Trans. B* (2002).

43. Gare, T. & Hazeldan, G. S. F. Basic oxygen steelmaking: decarburization of binary Fe-C droplets and ternary Fe-C-X droplets in ferruginous slags. *Ironmak. Steelmak.* **8,** 169–181 (1981).

44. Yin, H., Shibata, H., Emi, T. & Suzuki, M. 'In-situ' Observation of Collision, Agglomeration and Cluster Formation of Alumina Inclusion Particles on Steel Melts. *ISIJ Int.* **37,** 936–945 (1997).

45. Yin, H., Shibata, H., Emi, T. & Suzuki, M. Characteristics of Agglomeration of Various Inclusion Particles on Molten Steel Surface. *ISIJ Int.* **37,** 946–955 (1997).

46. Shibata, H., Arai, Y., Suzuki, M. & Emi, T. Kinetics of peritectic reaction and transformation in Fe-C alloys. *Metall. Mater. Trans. B* **31,** 981–991 (2000).

47. H. Shibata, T. Emi, H. Yin, M. S. Kinetics and morphology of crystal growth interacting with non-metalic inclusion in iron alloy melts. in *4th Decenn. Int. Conf. Solidif. Process.* **37,** 230–233 (1997).

48. Kumar, J., Attridge, A., Wood, P. K. C. & Williams, M. a. Analysis of the effect of cone-beam geometry and test object configuration on the measurement accuracy of a computed tomography scanner used for dimensional measurement. (2011). doi:10.1088/0957-0233/22/3/035105